Letter

Quantum Efficiency of III-Nitride Emitters: Evidence for Defect-Assisted Nonradiative Recombination and its Effect on the Green Gap

Aurelien David,* Nathan G. Young, Christophe A. Hurni, and Michael D. Craven
Soraa Inc., 6500 Kaiser Drive, Fremont, California 94555, USA

(Received 11 September 2018; revised manuscript received 5 December 2018; published 1 March 2019)

Carrier-lifetime measurements reveal that, contrary to common expectations, the high-current nonradiative recombination (droop) in III-nitride light emitters is comprised of two contributions that scale with the cube of the carrier density: an intrinsic recombination—most likely standard Auger scattering—and an extrinsic recombination that is proportional to the density of point defects. This second droop mechanism, which has not previously been observed, may be caused by an impurity-assisted Auger process. Further, it is shown that longer-wavelength emitters suffer from higher point-defect recombinations, in turn causing an increase in the extrinsic droop process. It is proposed that this effect leads to the green gap and that point-defect reduction is a strategy to both vanquish the green gap and more generally improve quantum efficiency at high current.

DOI: 10.1103/PhysRevApplied.11.031001

Although modern III-nitride light-emitting diodes (LEDs) can reach very high efficiency [1], they still suffer from two important limitations. First, their internal quantum efficiency (IQE) decreases at high current, an effect known as efficiency droop. It is by now generally believed that droop is, at least in part, caused by Auger scattering—owing to the approximately cubic dependence of the droop current on the carrier density [2,3] and the observation of Auger electrons [4]. Second, the IQE decreases at long wavelength (corresponding to a high In content in the active region), a phenomenon of controversial origin, known as the "green gap." Various explanations have been offered for the green gap. It has been proposed that high-In quantum wells (QWs) suffer from an increase in point defects [5,6]; however, this should only impact low-current recombinations, whereas the green gap occurs at all currents. Other tentative explanations include an increase in electron-hole separation (leading to weaker radiative recombinations), due to increasing polarization fields and in-plane carrier localization [7–9]. Crucially, these explanations do not clarify the role played by nonradiative recombinations in the green gap. The combined effects of droop and the green gap have made it challenging to achieve efficient long-wavelength LEDs at high current density, hindering important applications such as III-nitride red-green-blue emitters.

In this Letter, we show that these two phenomena are connected and propose a mechanism for the green gap. We investigate droop dynamics in detail and show that droop is in fact caused by a combination of two processes, one intrinsic and the other extrinsic and scaling with the point-defect concentration. We then confirm that a high In content leads to an increase in point-defect recombinations, which in turn leads to an increase of the extrinsic droop component and the appearance of the green gap.

We study samples with 4-nm-thick single QWs within p-i-n regions, grown on c-plane bulk GaN substrates by metal-organic chemical-vapor deposition; these samples include an (In,Ga)N underlayer (UL) beneath the p-i-n region, which improves the material quality [10–12]. Importantly, the QW is placed at the center of the intrinsic region to avoid modulation doping, which would alter the recombination dynamics [13].

We first summarize important properties of the recombination dynamics in (In,Ga)N QWs. We measure carrier lifetimes (τ) with an optical-differential-lifetime (ODL) technique under laser excitation, details of which can be found in Ref. [14]. ODL uniquely enables the measurement of lifetimes down to low current density—in the Shockley-Read-Hall (SRH) regime—and is devoid of electrical injection artifacts [15]. We obtain τ as a function of the optical current density (J) in the QW. Concurrently, we measure the sample's absolute IQE as follows: the geometry of the setup and the sample structure are designed to provide repeatable optical collection across samples, so that each sample's relative IQE is obtained directly from the luminescence intensity; absolute calibration is established by growing several pairs of samples, wherein one sample in the pair is used for ODL measurement and the other is processed as LEDs, the extraction efficiency of which is known [1,16], leading to an accurate

*aurelien.david@polytechnique.org

 © 2019 American Physical Society

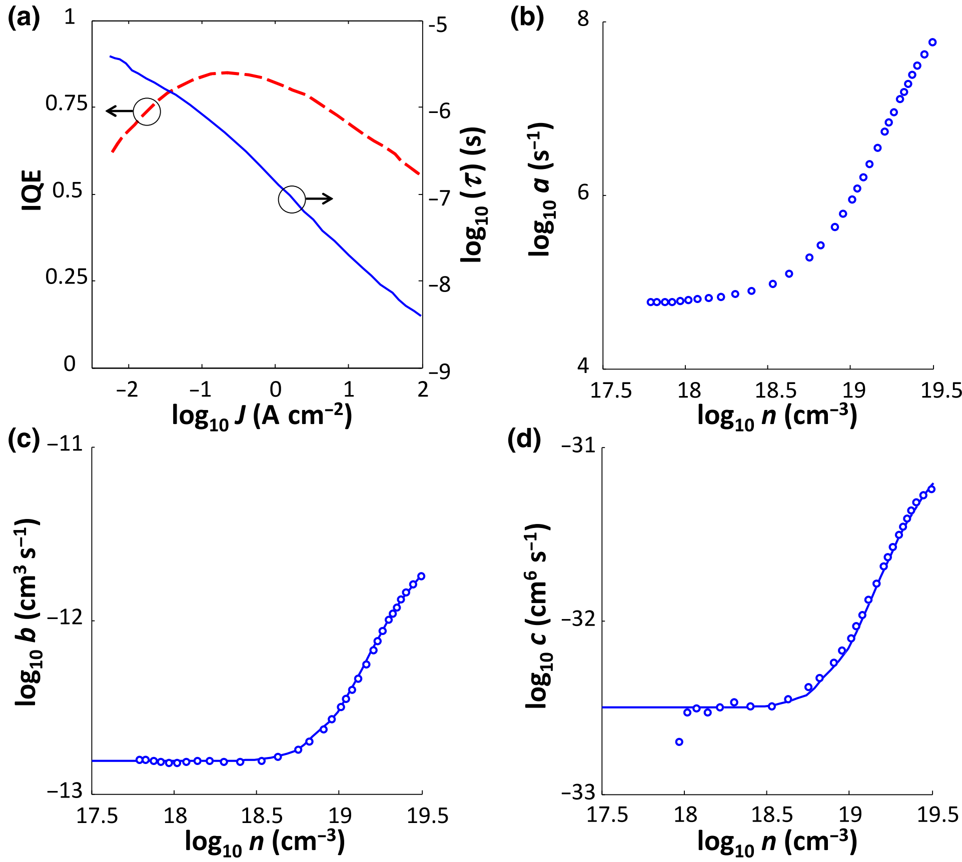

FIG. 1. The results from ODL measurements of a single-QW sample. (a) The lifetime (full line) and the IQE (dashed line). (b) The nonradiative component a, the low-current plateau of which gives the SRH coefficient A. (c) The radiative component b, showing the carrier dependence of the radiative recombinations: symbols, the experimental data; line, the empirical fit, from which the screening function S is derived (i.e., $b \sim S^2$). (d) The nonradiative component c, showing the carrier dependence of Auger scattering: symbols, the experimental data; line, the fit by $c \sim S^p$.

IQE determination. These coupled measurements of lifetime and IQE yield the carrier density (n) in the QW and the radiative and nonradiative rates (G_R, G_{NR}), from which we derive three important quantities:

$$a = G_{NR}/n, \quad b = G_R/n^2, \quad c = (G_{NR} - An)/n^3. \quad (1)$$

These quantities assume a simple interpretation in the framework of the well-known *ABC* model: at low current, a should be equal to the SRH coefficient A; while at all currents, b and c should be constant and, respectively, equal to the radiative coefficient B and the Auger coefficient C. For now, we place ourselves in this framework, although the interpretation of c will be refined hereafter. In practice, A is first extracted from the low-current plateau of a and this value is then subtracted in Eq. (1) to calculate c.

Experiments have shown that b and c are in fact current-dependent quantities [14]. As shown in Fig. 1 (for a sample with [In] = 13%), they increase with carrier density due to screening of the polarization field across the QW, which induces an increase of the electron-hole overlap $I = \int \psi_e \psi_h$. It is well known that $B \sim I^2$ [17]. Regarding Auger scattering, experiments and calculations have shown that $C \sim I^p$, with $p \approx 2$–3 [depending on the mixture of the electron-electron-hole (*eeh*) and electron-hole-hole (*ehh*) contributions] [14,18,19].

I can be decomposed according to $I(n) = I_0 S(n)$, where I_0 is the low-current value of I and S is a screening function accounting for the effect of carriers on the potential, with S normalized to unity at low current. Often, S is evaluated numerically from a simple one-dimensional (1D) Poisson-Schrödinger model, as was done in Ref. [14]; however, such computations are of limited accuracy as they ignore in-plane carrier localization. Instead, in this Letter, we derive S empirically from $S = \sqrt{b/B_0}$. The overlap dependence of C can then be explicitly verified, as shown in Fig. 1(d): we find that $p \approx 2.4$, indicating a mixture of *eeh* and *ehh* Auger processes. Thus, we have $b = B_0 S^2$ and $c = C_0 S^p$, with the low-current values (subscript 0) obtained before the onset of screening.

Further, we have shown in Ref. [20] that the coefficient A, derived from Eq. (1), also scales with wavefunction overlap. Indeed, both electrons and holes need to be present at a point defect to complete a SRH recombination cycle. Experimentally, we find $A \sim I^q$ with $q \approx 1.6$ [21].

In summary, all three recombination mechanisms scale with similar exponents of the overlap I. Thus, for various active regions spanning a large range of overlaps, these dependencies cancel out, leading to nearly constant peak IQE, as shown in Ref. [20].

Given this backdrop, we now study a series of samples where the SRH rate is intentionally varied by one of three

TABLE I. Details of the samples ("UL" refers to the relative thickness of the UL and the values of A and c_0 are on the $\log_{10}$ scale).

No.	Growth	UL (%)	ΔT	A (s^{-1})	c_0 ($cm^6\ s^{-1}$)
1	1	100	0	4.78	−32.49
2	2	100	0	5.44	−32.10
3	2	80	0	5.67	−31.96
4	2	50	0	6.38	−31.33
5	2	20	0	6.72	−31.07
6	2	0	0	7.21	−30.79
7	2	100	+150 °C	6.41	−31.33

methods. In a first case, we vary the epi growth between conditions labeled *1* and *2* (with *2* being comparatively worse); in a second case, we vary the UL thickness (with a thinner UL leading to a lower IQE); in a third case, we increase the growth temperature of the intrinsic GaN layer underneath the QW [22] by ΔT (leading to a lower IQE). Importantly, in all samples, the active region is identical, with [In] = 13%. Table I shows the details of the samples. Figure 2 shows each sample's IQE and quantities (b, c) determined from ODL measurements. Quantity a (not shown) displays a clear low-current plateau for each sample, from which A is extracted. The fact that an increase in growth temperature in a layer well below the active region leads to an increase in point defects (see sample 7), as previously noted in Ref. [12], suggests that the defect at play may be intrinsic rather than extrinsic.

The IQE varies significantly across the series. The samples with higher A suffer from a low IQE at low current, as expected. However, their high-current IQE is also impacted. This is surprising because SRH recombinations should have little influence beyond 100 A cm^{-2}. To illustrate this, we model the expected impact of increasing A while b and c remain unchanged for each sample (with values of b and c taken from the brightest sample). Figure 2(a) shows all modeled curves converging at high J, in contrast to the data. To explain this discrepancy, we turn our attention to the other recombination channels.

Figure 2(b) shows that b is nearly identical for all samples, indicating that the radiative rate is the same, which is as expected since they have the same active region. Incidentally, this confirms the accuracy of the ODL technique for measuring recombination rates, since all samples have markedly different lifetimes and IQEs, but the same b is derived from each one.

In contrast, in Fig. 2(c), c shows a strong variation (more than one order of magnitude) across the series: the samples with higher A also have higher c. This is unexpected if we simply attribute C to Auger scattering—an intrinsic process, which should be constant for all samples, just like radiative recombination. Instead, the interpretation of c has to be revised; the data lends itself to the following

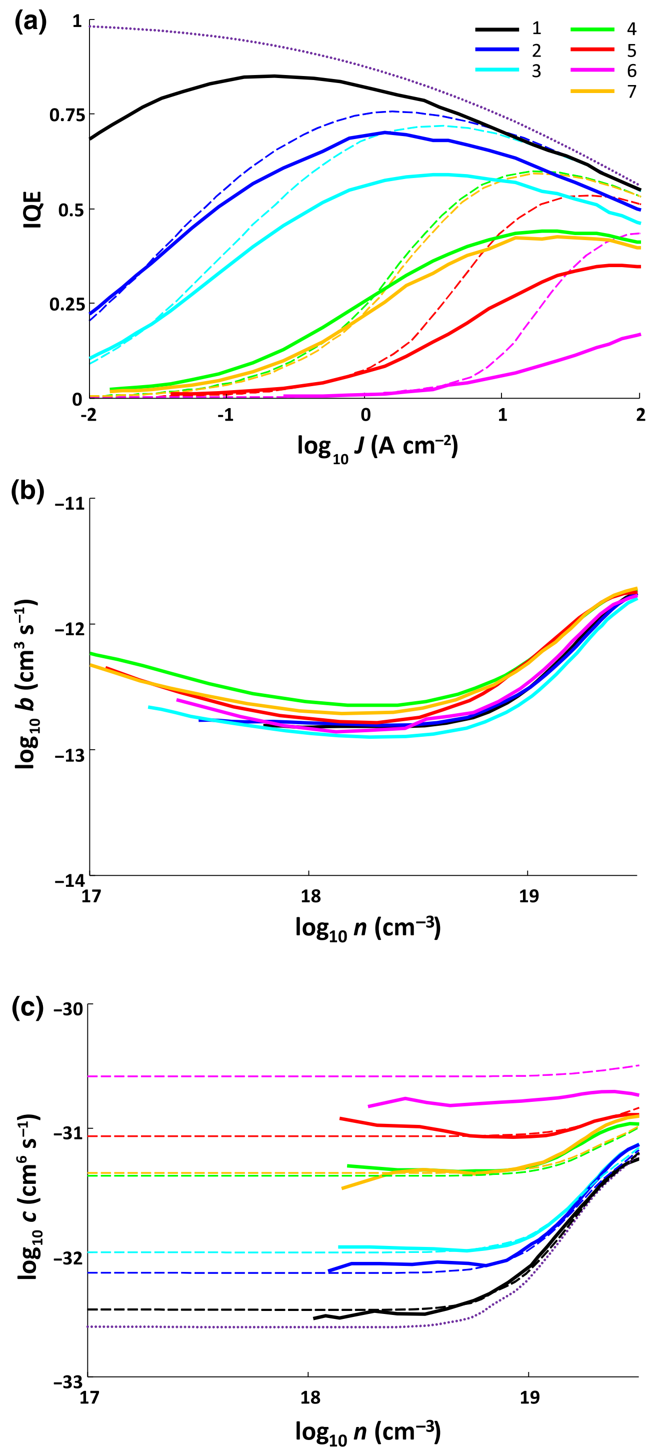

FIG. 2. ODL-derived results for the Table I samples. (a) Full lines, the experimental IQE; dashed lines, the modeled IQE for varying A but constant values of b and c (the model does not predict the decrease in IQE at high current); dotted line, the theoretical IQE limit in the intrinsic case ($A = 0$, $D = 0$). (b) The radiative term b is nearly identical for all samples. (c) The nonradiative term c (full lines) varies across the series: dashed lines, fits according to Eq. (2); dotted line, the intrinsic Auger component, resulting in the dotted line in (a).

decomposition:

$$c = C_0 S^p n^3 + D n^3, \quad (2)$$

where C_0 is an intrinsic Auger coefficient (constant for all samples) and D denotes a second, extrinsic, droop process *which scales with A*. This decomposition yields good fits for values of C_0 in the range (2–3) $\times 10^{-33}$ cm^6 s^{-1}. Hereafter, we use $C_0 = 2.5 \times 10^{-33}$ cm^6 s^{-1}, which leads to a close match to the experimental data [shown in Fig. 2(c)], from which we derive the value of D for each sample. It is worth noting that the two processes of Eq. (2) differ in their wave-function-overlap dependence (the intrinsic process increases at high density due to field screening, whereas the extrinsic process does not), which shows that the extrinsic process is not simply caused by an increase in magnitude of intrinsic Auger scattering.

Figure 3 shows the resulting correlation between A and D. The two coefficients are correlated with a slope on the log-log scale of about unity (the precise value depends on the assumed value of C_0, but remains in the range 0.8–1.2). We conclude that to first order, $D = kA$ with $k = 2 \times 10^{-38}$ cm^6. This linear relationship suggests a causal relationship between defects and extrinsic droop. Namely, for a given active region design, A is proportional to the concentration of a point defect causing SRH recombinations. D scales *linearly* with A, suggesting that this same point defect also induces an Auger-like nonradiative process, which adds to the intrinsic Auger scattering present in all samples. Only for sample 1, which has the lowest defect density, is the droop near the intrinsic limit indicated in Fig. 2. Crucially, this shows that defect reduction is essential for high-current performance.

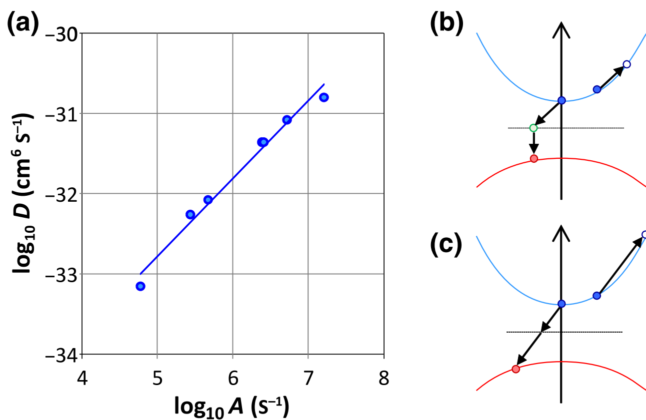

FIG. 3. (a) The correlation between the SRH coefficient A and the extrinsic droop coefficient D (on a log-log scale), with a slope of 1 ± 0.2. (b),(c) Band diagrams for possible high-order processes involving a trap: (b) electron Auger scattering into a trap followed by SRH hole recombination with the trap; (c) an *eeh* Auger process where the trap level acts as a virtual state.

Theoretical work has shown that the magnitude of the Auger coefficient in III-nitrides can be explained by considering phonon- and disorder-assisted processes [23,24]. Such microscopic processes are plausible explanations for the intrinsic droop current reported here. On the other hand, these processes do not involve defects and cannot account for the extrinsic droop component. Rather, they should be constant across samples, since the structure of the active region is unchanged.

Various high-order nonradiative mechanisms involving traps can be considered to account for the extrinsic process. However, its well-defined cubic dependence on the carrier density [manifested as clear plateaus across more than a decade in carrier density in Fig. 2(c)] imposes restrictions. Figure 3(b) shows a process often considered in other materials: a combination of an Auger scattering to a trap state [25,26] followed by an SRH recombination; it can be verified that such processes have a carrier dependence between n and n^2. More generally, processes generating a population in the trap state will deviate from an n^3 scaling. On the other hand, the mechanism of Fig. 3(c) (Auger scattering involving the trap level as a virtual state, without population buildup) would possess the proper carrier dependence and is a possible candidate—the magnitude of such a process in GaN has not been investigated. Qualitatively, defect states close to midgap (which are the likeliest source of SRH recombination) also reduce the energy threshold for Auger scattering, making such defect-assisted transitions plausible. Another possibility is enhancement of conventional Auger recombination by scattering at charged-defects, although this was investigated theoretically in Ref. [24] and predicted to be negligible (even for high charged-defect densities precluded in our samples). Non-Auger processes might even be considered, such as the density-activated SRH mechanism of Ref. [27] (however, that mechanism does not have a prescribed dependence on carrier density, making it a less natural explanation than an Auger process). Further theoretical exploration would be warranted to determine which specific process may account for our observations.

To explore the broader implications of this extrinsic droop process, we now consider samples of varying QW composition in the range [In] = 8%−25%; i.e., spanning the violet-to-green range [28]. We grow series of such samples using epi conditions *1* and *2* mentioned above (and a full UL thickness of 100%). The study comprises 44 samples, whose values of A, B_0, and $c_0 = C_0 + D$ are measured by ODL and shown in Fig. 4. Their peak IQE is roughly constant in the violet-blue range (for a given epi condition) but decreases at longer wavelength—a manifestation of the green gap. The radiative rate is well behaved, with Fig. 4(b) showing that B_0 decreases with higher [In], as anticipated due to the decreasing wave-function overlap and regardless of the epi growth conditions.

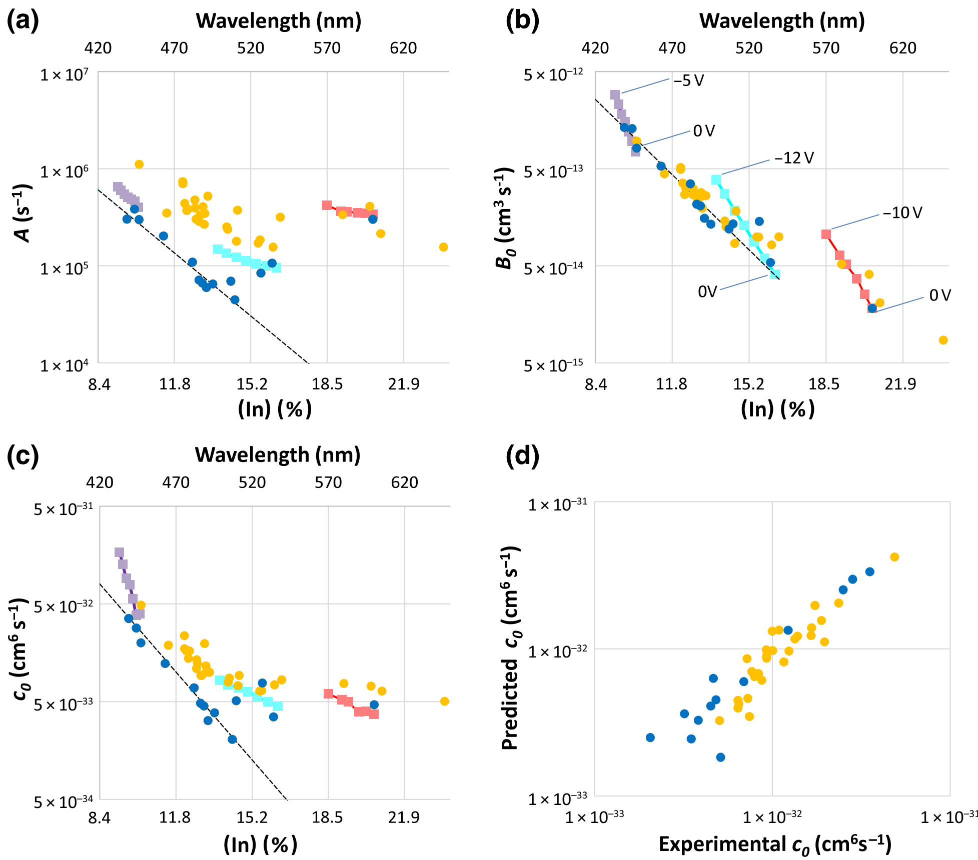

FIG. 4. (a)–(c) The recombination coefficients A, B_0, and c_0, plotted as a function of the emission wavelength and the corresponding [In]. The symbols represent the following: dots, samples of varying composition (blue dots, epi condition *1*; yellow dots, epi condition *2*); dashed lines, empirical wave-function dependencies $A \sim I^q$ ($q = 1.6$), $B \sim I^2$, and $C \sim I^p$ ($p = 2.3$); full lines with squares, samples under reverse bias (purple, cyan, and red indicate [In] = 10%, 16%, and 22%, respectively). The bias endpoints are indicated on (b). (d) The correlation between the measured value of c_0 and the predicted value according to Eq. (2).

Next, we consider A [Fig. 4(a)], which we expect to scale with both the defect density and the wave-function overlap. Indeed, for moderate QW compositions ([In] = 8%–15%), A decreases with [In]—the trend is clearest in samples with epi condition *1*, but is also observed with condition *2* (albeit with higher values of A and more variability). This corresponds to the aforementioned regime, where the point-defect incorporation remains constant and variations in A are driven by wave-function overlap (i.e., $A \sim I^q$). However, for higher [In], this trend breaks down and A remains roughly constant as the QW composition increases. This marks a departure from the previous regime and indicates that either (i) the point-defect density increases with [In] and/or (ii) the overlap dependence of A is altered.

Remarkably, the trend for the droop coefficient $c_0 = C_0 + D$ closely follows that of A. For a given growth condition, c_0 first decreases with overlap before reaching an approximate plateau. We propose that the departure of c_0 from the intrinsic regime I^p is driven by variations in point defects and hence D. To verify this, we show in Fig. 4(d) the values of c_0 predicted by Eq. (2)—these closely match the experiment, confirming a systematic coupling between SRH defects and extrinsic droop.

To further understand the behavior of A and c_0, we perform additional ODL measurements with a reverse bias applied to the samples. The bias reduces the electric field across the QW [29] and the resulting quantum-confined Stark effect, enabling a direct measurement of the overlap dependence of recombinations in a given sample. We measure three samples with [In] = 10%, 16%, and 22% (note that a reverse-bias photocarrier leakage current is observed for the 10% sample [30]; this effect is corrected-for in the data analysis). The results are included in Fig. 4, using the samples' wavelength to superimpose the data with the previous experiment. The bias-induced increase in overlap leads to a well-behaved increase in B_0 for all samples (the wavelength dependence of these curves is slightly different from that of the previous experiment: this is because it is induced by a change in field, rather than composition). In contrast, the overlap dependence of A is most pronounced for the low-content sample and nearly nonexistent for the high-content sample. Accordingly, c_0 shows a similar behavior.

Thus, as the QW's indium content increases, there is a transition from a "well-behaved" regime where all recombinations have pronounced overlap dependence [following the dashed lines in Fig. 4] to the green-gap regime where A and c_0 become nearly constant (overlap independent). This transition might be due to the formation of a different SRH-causing defect or to a change in the physics governing SRH recombinations in high-composition QWs. We hypothesize that increased carrier localization in high-content samples may contribute to these observations.

In summary, we show two crucial results for understanding the efficiency of III-nitride LEDs. First, droop has two contributions. In addition to the known intrinsic Auger scattering in low-defect materials, SRH-causing defects also induce an additional extrinsic Auger-like nonradiative process, which dominates droop in high-defect materials—in stark contrast to the common expectation that droop and defects are independent. Second, in long-wavelength samples with a high In content, SRH recombinations become weakly dependent on the wave-function overlap and their value remains constant. Correspondingly, the extrinsic droop process remains constant while the radiative rate is reduced—a trend that has been overlooked in previous studies focusing solely on radiative dynamics. We propose that this unfavorable balance of recombinations causes the green gap and that improvements in long-wavelength III-nitride emitters *at all currents* may be enabled by a reduction in SRH defects and the associated droop process.

[1] C. A. Hurni, A. David, M. J. Cich, R. I. Aldaz, B. Ellis, K. Huang, A. Tyagi, R. A. DeLille, M. D. Craven, and F. M. Steranka, Bulk GaN flip-chip violet light-emitting diodes with optimized efficiency for high-power operation, Appl. Phys. Lett. **106**, 031101 (2015).

[2] Y. C. Shen, G. O. Mueller, S. Watanabe, N. F. Gardner, A. Munkholm, and M. R. Krames, Auger recombination in InGaN measured by photoluminescence, Appl. Phys. Lett. **91**, 141101 (2007).

[3] A. David and M. J. Grundmann, Droop in InGaN light-emitting diodes: A differential carrier lifetime analysis, Appl. Phys. Lett. **96**, 103504 (2010).

[4] J. Iveland, L. Martinelli, J. Peretti, J. S. Speck, and C. Weisbuch, Direct Measurement of Auger Electrons Emitted from a Semiconductor Light-Emitting Diode under Electrical Injection: Identification of the Dominant Mechanism for Efficiency Droop, Phys. Rev. Lett. **110**, 177406 (2013).

[5] A. M. Armstrong, M. H. Crawford, and D. D. Koleske, Contribution of deep-level defects to decreasing radiative efficiency of InGaN/GaN quantum wells with increasing emission wavelength, Appl. Phys. Express **7**, 032101 (2014).

[6] S. Hammersley, M. J. Kappers, F.-P. Massabuau, S. L. Sahonta, P. Dawson, R. A. Oliver, and C. J. Humphreys, Effects of quantum well growth temperature on the recombination efficiency of InGaN/GaN multiple quantum wells that emit in the green and blue spectral regions, Appl. Phys. Lett. **107**, 132106 (2015).

[7] S. Schulz, M. A. Caro, C. Coughlan, and E. P. O'Reilly, Atomistic analysis of the impact of alloy and well-width fluctuations on the electronic and optical properties of InGaN/GaN quantum wells, Phys. Rev. B **91**, 035439 (2015).

[8] M. Auf der Maur, A. Pecchia, G. Penazzi, W. Rodrigues, and A. Di Carlo, Efficiency Drop in Green InGaN/GaN Light Emitting Diodes: The Role of Random Alloy Fluctuations, Phys. Rev. Lett. **116**, 027401 (2016).

[9] F. Nippert, S. Y. Karpov, G. Callsen, B. Galler, T. Kure, C. Nenstiel, M. R. Wagner, M. Strassburg, H.-J. Lugauer, and A. Hoffmann, Temperature-dependent recombination coefficients in InGaN light-emitting diodes: Hole localization, Auger processes, and the green gap, Appl. Phys. Lett. **109**, 161103 (2016).

[10] T. Akasaka, H. Gotoh, T. Saito, and T. Makimoto, High luminescent efficiency of InGaN multiple quantum wells grown on InGaN underlying layers, Appl. Phys. Lett. **85**, 3089 (2004).

[11] C. Haller, J. F. Carlin, G. Jacopin, D. Martin, R. Butte, and N. Grandjean, Burying non-radiative defects in InGaN underlayer to increase InGaN/GaN quantum well efficiency, Appl. Phys. Lett. **111**, 262101 (2017).

[12] C. Haller, J. F. Carlin, G. Jacopin, W. Liu, D. Martin, R. Butte, and N. Grandjean, GaN surface as the source of non-radiative defects in InGaN/GaN quantum wells, Appl. Phys. Lett. **113**, 111106 (2018).

[13] T. Langer, A. Chernikov, D. Kalincev, M. Gerhard, H. Bremers, U. Rossow, M. Koch, and A. Hangleiter, Room temperature excitonic recombination in GaInN/GaN quantum wells, Appl. Phys. Lett. **103**, 202106 (2013).

[14] A. David, N. G. Young, C. A. Hurni, and M. D. Craven, All-optical measurements of carrier dynamics in bulk-GaN LEDs: Beyond the ABC approximation, Appl. Phys. Lett. **110**, 253504 (2017).

[15] A. David, C. A. Hurni, N. G. Young, and M. D. Craven, Carrier dynamics and Coulomb-enhanced capture in III-nitride quantum heterostructures, Appl. Phys. Lett. **109**, 033504 (2016).

[16] A. David, C. A. Hurni, R. I. Aldaz, M. J. Cich, B. Ellis, K. Huang, F. M. Steranka, and M. R. Krames, High light extraction efficiency in bulk-GaN based volumetric violet light-emitting diodes, Appl. Phys. Lett. **105**, 231111 (2014).

[17] G. Lasher and F. Stern, Spontaneous and stimulated recombination radiation in semiconductors, Phys. Rev. **133**, A553 (1964).

[18] A. David and M. J. Grundmann, Influence of polarization fields on carrier lifetime and recombination rates in InGaN-based light-emitting diodes, Appl. Phys. Lett. **97**, 033501 (2010).

[19] C. M. Jones, C.-H. Teng, Q. Yan, P.-C. Ku, and E. Kioupakis, Impact of carrier localization on recombination in InGaN quantum wells and the efficiency of nitride light-emitting diodes: Insights from theory and numerical simulations, Appl. Phys. Lett. **111**, 113501 (2017).

[20] A. David, C. A. Hurni, N. G. Young, and M. D. Craven, Field-assisted Shockley-Read-Hall recombinations in III-nitride quantum wells, Appl. Phys. Lett. **111**, 233501 (2017).

[21] This exponent is slightly different from the value $q = 1.3$ that we found in Ref. [20]. This is because the former exponent was derived from a 1D Poisson-Schrödinger model of I, whereas here we evaluate I empirically from $I \sim \sqrt{B}$.

[22] More precisely, the first half of this layer is grown hot; the second half is grown at normal temperature, to ensure good morphology before growing the QW.

[23] E. Kioupakis, P. Rinke, K. T. Delaney, and C. G. Van de Walle, Indirect Auger recombination as a cause of

efficiency droop in nitride light-emitting diodes, Appl. Phys. Lett. **98**, 161107 (2011), times Cited: 20 161107.

[24] E. Kioupakis, D. Steiauf, P. Rinke, K. T. Delaney, and C. G. Van de Walle, First-principles calculations of indirect Auger recombination in nitride semiconductors, Phys. Rev. B **92**, 035207 (2015).

[25] P. T. Landsberg, C. Rhys-Roberts, and P. Lal, Auger recombination and impact ionization involving traps in semiconductors, Proc. Phys. Soc. **84**, 915 (1964).

[26] J. G. Fossum, R. P. Mertens, D. S. Lee, and J. F. Nijs, Carrier recombination and lifetime in highly doped silicon, Solid State Electron. **26**, 569 (1983).

[27] J. Hader, J. V. Moloney, and S. W. Koch, Density-activated defect recombination as a possible explanation for the efficiency droop in GaN-based diodes, Appl. Phys. Lett. **96**, 221106 (2010).

[28] In this study, the high-In samples emit at long wavelength at low current (see Fig. 4) due to the strong QW-polarization fields in our test structures. At higher current, the wavelength shifts to a more typical value due to field screening.

[29] U. T. Schwarz, H. Braun, K. Kojima, Y. Kawakami, S. Nagahama, and T. Mukai, Interplay of built-in potential and piezoelectric field on carrier recombination in green light emitting InGaN quantum wells, Appl. Phys. Lett. **91**, 123503 (2007).

[30] A. David and N. F. Gardner, Droop in III-nitrides: Comparison of bulk and injection contributions, Appl. Phys. Lett. **97**, 193508 (2010).